CMS Physics Analysis Summary

Contact: cms-pag-conveners-susy@cern.ch 2016/10/11

Search for natural supersymmetry in events with top quark pairs and photons in pp collisions at $\sqrt{s} = 8$ TeV

The CMS Collaboration

Abstract

We present a search for a natural gauge-mediated supersymmetry breaking scenario with the top squark as the lightest squark and the gravitino as the lightest supersymmetric particle. The strong production of top squark pairs and their decays would produce events with pairs of top quarks and neutralinos, with each neutralino decaying to a photon and a gravitino. This search is performed with the CMS experiment using pp collision data at $\sqrt{s} = 8$ TeV, corresponding to an integrated luminosity of 19.7 fb^{-1}, in the electron + jets and muon + jets channel, requiring one or two photons in the final state. We compare the missing transverse momentum of these events against the expected spectrum of standard model processes. No excess of events is observed beyond background predictions and the result of the search is interpreted in the context of a general model of gauge-mediated supersymmetry breaking deriving limits on the mass of top squarks up to 750 GeV.

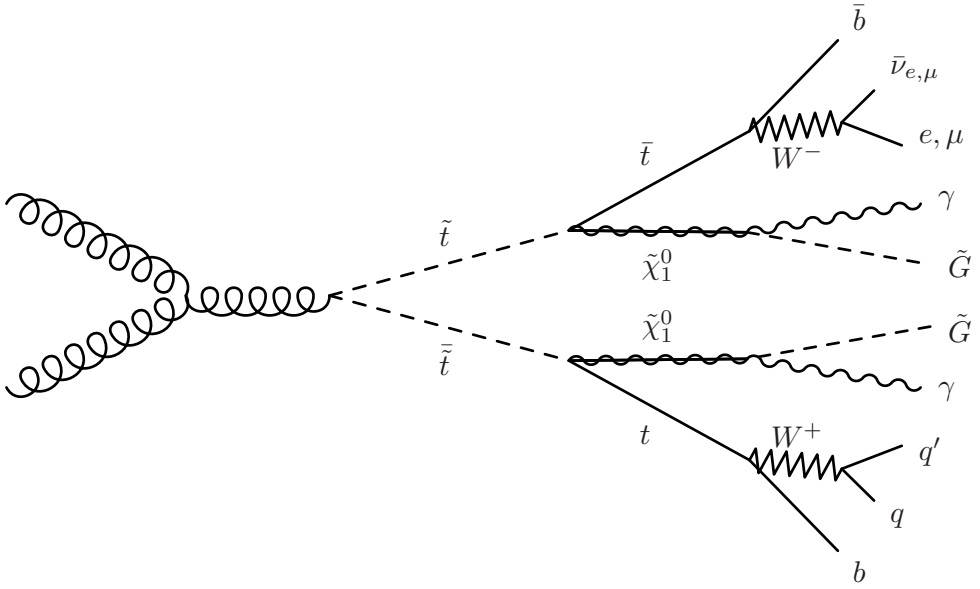

Figure 1: Feynman diagram of the GMSB scenario of interest. With top squarks as the lightest squark, the pair production of stops would be the dominant production mechanism for SUSY in pp collisions at the LHC. Assuming a bino-like neutralino NLSP, each stop would decay to a top quark and a neutralino, with the neutralino decaying to a photon and gravitino. Shown above is the electron + jets or muon + jets final state of the top pair decay.

1 Introduction

Supersymmetry (SUSY) [1–9] is increasingly desirable in avoiding the hierarchy problem of the recently-discovered Higgs boson at 125 GeV [10–14]. Of particular interest are so-called "natural" models of SUSY in which, for standard model particles with large couplings to the Higgs boson, their supersymmetric partners (sparticles) are kept light, namely the third-generation squarks and electroweak gauginos [15, 16]. Such regions of SUSY parameter space would avoid introducing a new little hierarchy problem [17], and have been left largely unexplored at the CERN LHC.

In this article we describe a search motivated by models of gauge-mediated supersymmetry breaking (GMSB) [18–23] in which the neutralino ($\tilde{\chi}_1^0$) is the next-to-lowest mass sparticle (NLSP) and the gravitino ($\tilde{G}$) is the lowest-mass sparticle (LSP). The gravitino escapes undetected and contributes to missing transverse momentum ($\vec{p}_{\mathrm{T}}^{\,\mathrm{miss}}$) in the detector, where the magnitude of $\vec{p}_{\mathrm{T}}^{\,\mathrm{miss}}$ is referred to as $E_{\mathrm{T}}^{\mathrm{miss}}$. This search considers the case of a bino-like neutralino, where photons in the final state originate from its $\tilde{\chi}_1^0 \rightarrow \gamma\tilde{G}$ decay. Assuming that R parity [24, 25] is conserved, pair production of strongly-interacting sparticles would be the dominant production mechanism for SUSY in pp collisions at the LHC. Further assuming that only the top squark (stop) is light enough to be producable at the LHC, SUSY production would proceed as pairs of top squarks decaying predominantly to a $t\bar{t} + \gamma\gamma + E_{\mathrm{T}}^{\mathrm{miss}}$ event topology, shown in Figure 1.

The analysis focuses on the semileptonic decay mode of the $\mathrm{t\bar{t}}$ pair, where one of the resulting W bosons decays to a lepton and neutrino. Based on 19.7 fb^{-1} of pp collisions at $\sqrt{s} = 8$ TeV, the analysis requires the presence of exactly one isolated lepton (either an electron or a muon) to avoid contributions from QCD multijet and γ+jet backgrounds and to enhance the semileptonic mode of $\mathrm{t\bar{t}}$ decays. At least one jet in each event is required to be tagged as originating from a b quark to further reduce non-$\mathrm{t\bar{t}}$ backgrounds. Two signal regions are defined for both electron

and muon channels depending on the number of selected photons in each event: either exactly one photon, or two photons. Control regions are similarly defined using photons that fail either the nominal isolation or shower shape requirements, referred to as misidentified photons.

The results of the analysis are evaluated by comparing the shape of the $E_{\mathrm{T}}^{\mathrm{miss}}$ distributions for the observed data and estimated backgrounds in the one and two photons signal regions. To reduce the dependance on the $t\bar{t}+\gamma\gamma$ production cross section, the $t\bar{t}+jets$ and $t\bar{t}+\gamma$ background normalizations are allowed to float freely to make the results a purely shape-based comparison. The results are interpreted against a range of stop and bino masses in a general gauge-mediated [26–31] (GGM) SUSY scenario.

2 The CMS Detector

The central feature of the CMS detector is a superconducting solenoid with an internal diameter of 6 m, providing a magnetic field of 3.8 T. Within its field volume are a silicon pixel and strip tracker, a lead tungstate crystal electromagnetic calorimeter (ECAL), and a brass and scintillator sampling hadron calorimeter (HCAL), each separated into barrel and endcap sections. The muon system, embedded in the steel return yoke outside of the solenoid, measures muons using drift tubes, cathode strip chambers, and resistive plate chambers. Extensive forward calorimetry compliments the coverage provided by the barrel and endcap detectors.

In the barrel section of the ECAL, an energy resolution of about 1% is achieved for unconverted or late-converting photons. The remaining barrel photons have a resolution of about 1.3% up to a pseudorapidity of $|\eta| = 1$, rising to about 2.5% at $|\eta| = 1.4$ [32]. Only photons in the barrel ECAL are considered by the analysis.

The missing transverse momentum vector $\vec{p}_{\mathrm{T}}^{\mathrm{miss}}$ is defined as the projection on the plane perpendicular to the beams of the negative vector sum of the momenta of all reconstructed objects in an event.

The first level of the CMS trigger system, composed of custom hardware processors, uses information from the calorimeters and muon detectors to select the most interesting events in a fixed time interval of less than 4 μs. The High Level Trigger (HLT) processor farm further decreases the event rate from around 100 kHz to about 400 Hz, before data storage.

A more detailed description of the CMS detector, together with a definition of the coordinate system used and the relevant kinematic variables such as pseudorapidity η or the azimuthal angle ϕ, can be found in Ref. [33].

3 Event and Object Reconstruction

All objects in the event (photons, electrons, muons, jets, and $E_{\mathrm{T}}^{\mathrm{miss}}$) are reconstructed using the particle flow (PF) algorithm [34–36]. Jets are reconstructed by clustering PF particles using the anti-k_T algorithm [37] with FastJet [38]. Jets use a distance parameter of 0.5 in the η-ϕ plane ($\Delta R = \sqrt{\Delta\phi^2 + \Delta\eta^2}$), and their momenta are corrected for the effects of multiple interactions in the same bunch crossing (pileup). All particle flow candidates are used to calculate $E_{\mathrm{T}}^{\mathrm{miss}}$.

Photons are reconstructed from clusters in the ECAL barrel with $|\eta| < 1.44$ and required to be tightly isolated having $p_T > 20$ GeV. The ratio of the energy deposit in the HCAL tower closest to the seed of the ECAL supercluster assigned to the photon divided by the energy deposit in the ECAL has to be smaller than 5%. A photon-like shower shape is required [32]. The isolation

energy is calculated in a cone with an outer radius of $\Delta R = 0.3$, where the imprint of the photon is removed. Pileup corrections depending on η are applied to all isolation energies.

Muons are reconstructed from measurements in the muon system and compatible track segments in the silicon tracker [39]. Candidate muons are required to have $p_T > 30$ GeV, be within $|\eta| < 2.1$, and have an isolation energy in a cone of radius $\Delta R = 0.4$ of less than 12% of their transverse momenta. Electrons are reconstructed from clusters of deposited energy in the ECAL, which are matched to a track in the silicon tracker [40]. Candidate electrons are required to have $p_T > 30$ GeV, be within $|\eta| < 2.5$, excluding the transition region between the ECAL barrel and endcap, and have an isolation energy in a cone of radius $\Delta R = 0.3$ less than 10% of their transverse momenta. An additional, looser requirement for each lepton provides a veto against dileptonic backgrounds.

The Combined Secondary Vertex algorithm [41] at the medium working point (CSVM) is used to identify jets from b quarks, increasing the signal sensitivity. The CSV algorithm uses secondary vertices and track impact parameters to provide a discriminant separating bottom-quark jets from charm, light quark, or gluon jets. The efficiency of the CSVM is around 70% for b-quark jets and 20% for c-quark jets. The efficiency of accidentally tagging light or gluon jets by this working point is around 2%.

4 Analysis Strategy

Events are required to pass a single electron (muon) trigger requiring an isolated electron (muon) with a minimum transverse momentum of 27 GeV (24 GeV). The single muon trigger additionally requires the muon candidate to be within $|\eta| < 2.1$.

Events are required to have exactly one candidate electron or muon. Events containing additional leptons satisfying a looser criteria of $p_T > 10$ GeV, $|\eta| < 2.5$, and isolation energy sums less than 20% of their transverse momenta are rejected. At least three jets with $p_T > 30$ GeV and $|\eta| < 2.4$ are required, and at least one jet must be tagged as from a b quark by the CSVM b tagger. All objects are required to be separated from each other by at least a ΔR of 0.5.

After this preselection, events are separated into independant samples based on the number of candidate photons selected. Candidate photons are required to be separated from all jets by at least a ΔR of 0.7. Two signal regions are defined: SR1 contains exactly one photon candidate, and SR2 contains two photon candidates.

Reconstructed photons that fail either the shower shape or charged hadron isolation energy sum requirements are referred to as misidentified photons. These objects are predominantly jets with large electromagnetic fluctuations in their hadronization and are used to define two control regions, similarly to the signal regions: CR1 contains exactly one misidentified photon and zero candidate photons, and CR2 contains two or more misidentified photons and zero candidate photons. The control region definition is chosen to not intersect with the signal regions, to have very low signal acceptance, and to greatly enhance the population of the photon-like jets contributing the most to the background estimate in the signal regions. The control regions allow for the study of the performance of the E_T^{miss} simulation with the most poorly reconstructed photon-like objects expected in the signal region, for which the effect on the E_T^{miss} resolution is expected to be much smaller than that of the presence of a semileptonic $t\bar{t}$ decay.

The background expected in the signal regions is largely dominated by $t\bar{t} + jets$ and $t\bar{t} + \gamma$ events where many selected photons originate from misreconstructed jets. These two processes

Table 1: Scale factors for the normalization of $Z(\gamma) + jets$ backgrounds and electron-to-photon misidentification rate. For the electron+jets channel, the product of the two is applied to $Z + jets$ and $W/Z + \gamma$ backgrounds. For the muon+jets channel, only the first one is applied. The uncertainties displayed are statistical followed by all systematic uncertainties added in quadrature.

Channel	$SF_{Z(\gamma)}$	$SF_{e\to\gamma}$
e	$1.38 \pm 0.02 \pm 0.15$	$1.58 \pm 0.03 \pm 0.04$
μ	$1.60 \pm 0.02 \pm 0.17$	–

are modeled in Monte Carlo (MC) simulations using the MADGRAPH 5.1.3 [42] tree-level matrix element generator matched to PYTHIA 6 [43] for the parton shower. Simulated $t\bar{t} + \gamma$ events were generated in a $2 \to 7$ configuration ($pp \to bbjj\ell\nu\gamma$ or any other WW final state). Approximately 0.6% of the simulated $t\bar{t} + jets$ events contain generator-level photon radiation falling into the defined phase space of the $t\bar{t} + \gamma$ sample and are rejected. Most other backgrounds are simulated with MADGRAPH and matched to PYTHIA, including $W/Z + jets$, single top, $t\bar{t} + W/Z$, and $W/Z + \gamma$ processes. Single top quark events are generated with POWHEG [44], modeling the decay of tau leptons with TAUOLA [45]. The Z2 tune [46] is used for the underlying event. All simulated backgrounds are normalized to the integrated luminosity of the data using their respective cross sections calculated at least at next-to-leading order.

The $Z + jets$ and $W/Z + \gamma$ backgrounds are small in the muon+jets channel. However in the electron+jets channel there is considerable misidentification of electrons as photons causing these processes to contribute appreciably to the signal regions at low $E_{\mathrm{T}}^{\mathrm{miss}}$. This misidentification rate is observable as the Z boson mass resonance in the invariant mass distribution of electron-photon pairs in the electron+jets channel of SR1. The measurement of this rate depends on the accurate estimation of the number of selected Z bosons in each channel. The first step is in measuring a scale factor for the $Z + jets$ and $Z\gamma + jets$ MC. This scale factor is measured using a dileptonic selection similar to the electron+jets SR1 selection, but altered to require two leptons of the same flavor instead of only one. Additional third leptons are still vetoed, and no photons are required. A template fit of the invariant mass of the dilepton system in data, using the $Z(\gamma) + jets$ MC as the signal template and all other MC as the background template, gives a normalization scale factor for the $Z(\gamma) + jets$ MC, labelled $SF_{Z(\gamma)}$.

Once this first scale factor has been applied to correct the MC estimate of the number of Z bosons, the Z resonance in the electron+jets channel of SR1 is used to derive a second scale factor $SF_{e\to\gamma}$ to correct the misdentification rate of electrons as photons. A template fit of the invariant mass of the electron-photon system in SR1 data, with $E_{\mathrm{T}}^{\mathrm{miss}} < 50$ GeV required to limit signal presence, is performed using the $Z(\gamma) + jets$ MC as the signal template and all other MC as the background template. Generator-level matching of reconstructed photons to generated electrons is applied to increase the purity of the misidentified $e\gamma$ mass template. To increase statistics in each template, the b tag requirement is removed for both MC and data selections as the misidentification rate does not depend on the presence of a b jet. From the result of this fit, a normalization scale factor is measured and applied to the $Z(\gamma) + jets$ MC in the electron signal regions. This second scale factor is not applied to the muon signal regions, as the misidentification rate of muons as photons is negligable. The results of the fits for each of these two scale factors are shown in Figure 2 and the obtained scale factors are listed in Table 1.

A final concern for the background estimate is in the simulation of the photon purity, or the relative compositions of photons and photon-like jets in the dominant $t\bar{t} + jets$ and $t\bar{t} + \gamma$ backgrounds. No explicit $t\bar{t} + \gamma\gamma$ sample is used in the background estimate due to the exceedingly small cross section for such events. As such the source of two photon events in SR2 will be lower-energy QED radiation and jets misidentified as photons. While the precise photon pu-

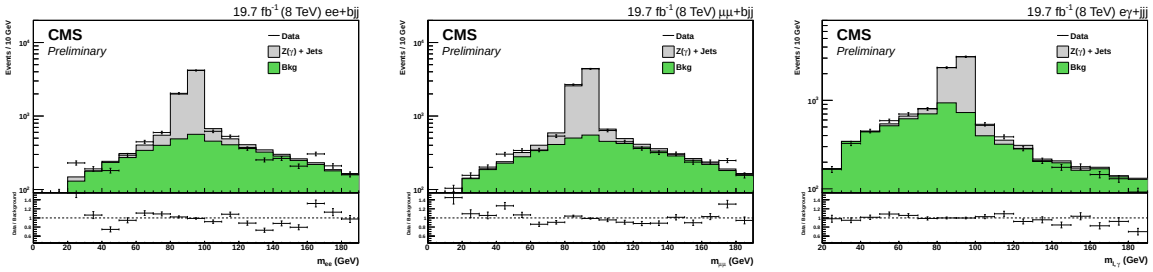

Figure 2: Template fit results for the dilepton invariant mass in deriving $SF_{Z(\gamma)}$ for the electron (left) and muon (middle) channels. The template fit result for $SF_{e\to\gamma}$ in $m_{e\gamma}$ for the electron channel in SR1 with the b tag requirement removed is shown on the right. The ratio of data to the total background is included at the bottom of each figure. Uncertainties shown are statistical only.

rity in each signal region is important for absolute rate measurements, no difference in the overall distribution of simulated $E_{\mathrm{T}}^{\mathrm{miss}}$ is found when altering the purity of selected photons. The maximal bin-by-bin difference between the simulated $E_{\mathrm{T}}^{\mathrm{miss}}$ of $t\bar{t}+jets$ and $t\bar{t}+\gamma$ events is found to be 5%. When their relative normalizations are adjusted to the observed photon purity in data by a template fit in photon isolation energy, this difference in shape is only 1-2%–well contained within statistical uncertainties on the total $E_{\mathrm{T}}^{\mathrm{miss}}$ shape. In short, the $E_{\mathrm{T}}^{\mathrm{miss}}$ distribution in both signal regions is found to be insensitive to the source of selected photons in $t\bar{t}+jets$ and $t\bar{t}+\gamma$ backgrounds, and as such no dedicated $t\bar{t}+\gamma\gamma$ sample is required. To eliminate any dependance on the overall production rate of $t\bar{t}+\gamma(\gamma)$ events, the $t\bar{t}+jets$ and $t\bar{t}+\gamma$ backgrounds are allowed to float freely in the upper limit calculations so that the interpretation of the results is completely shape-based.

With the above scale factors applied to each background, the control regions offer a signal-free evaluation of the performance of the $E_{\mathrm{T}}^{\mathrm{miss}}$ background shape prediction, giving an acceptance times efficiency of less than 1% of the signal model. By inverting the photon shower shape or charged hadron isolation energy sum requirements, CR1 and CR2 contain the same $\mathrm{t\bar{t}}$ system as the signal regions but greatly enhance the contribution of misidentified jets in the photon system of each event. The observed data and predicted background $E_{\mathrm{T}}^{\mathrm{miss}}$ shape is shown in Figure 3 for each control region. The agreement between data and MC is good, considering the very limited statistics available in CR2.

As an estimate of the performance of the $E_{\mathrm{T}}^{\mathrm{miss}}$ shape in the signal regions, the bin-by-bin difference in CR1 for each channel is taken as a percentage systematic uncertainty in the signal regions. CR2 is statistically limited and cannot indicate systematic differences over statistical fluctuations. Thus CR1 is used for both SR1 and SR2 for this purpose. Additional systematic uncertainties are applied due to the differences in shape between CR1 and the signal regions, calculated as the bin-by-bin ratio of signal region to control region $E_{\mathrm{T}}^{\mathrm{miss}}$ distributions. Overall this accounts for a 10–20% shape systematic due to the data-to-MC difference in CR1, a 1–8% shape systematic due to the difference in shape between CR1 and SR1, and a 10–50% shape systematic (the 50% value applies only in the highest $E_{\mathrm{T}}^{\mathrm{miss}}$ bin) for only SR2 due the difference in shape between SR1 and SR2.

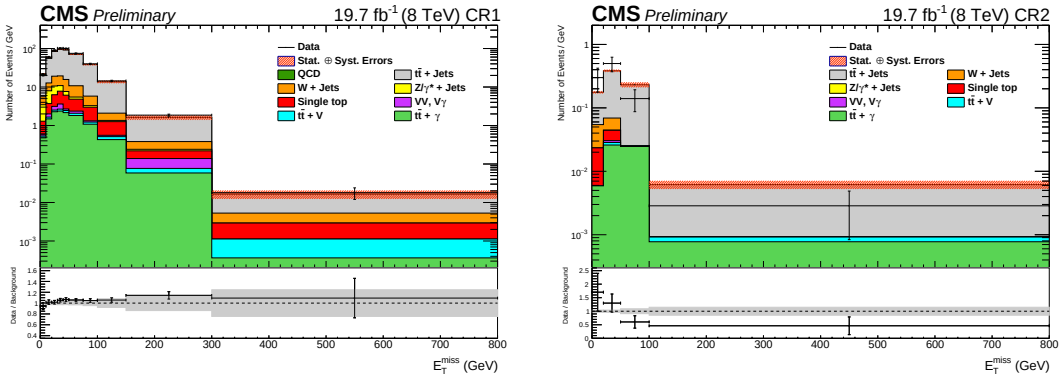

Figure 3: Comparison of data and MC in $E_{\mathrm{T}}^{\mathrm{miss}}$ for the combined (e+μ) control regions. Both CR1 (left) with one misidentified photon and CR2 (right) with two misidentified photons are shown. The disagreement of 10–20% between data and MC in CR1 is taken as an additional shape-based systematic uncertainty in the signal regions. The comparitively poor agreement in CR2 is attributable to the very small number of events in data and is not taken as an additional uncertainty.

Table 2: Summary of systematic uncertainties considered. The dominant rate uncertainty is the $t\bar{t}+\gamma$ and $V\gamma$ normalizations, although the $t\bar{t}+jets$ and $t\bar{t}+\gamma$ backgrounds are allowed to float freely in the upper limit determination. Check marks indicate uncertainties that affect the shape of the $E_{\mathrm{T}}^{\mathrm{miss}}$ distribution in addition to overall rates. The dominant shape uncertainties are the control region-derived uncertainties.

Source	Shape	Rate	Notes
Luminosity		2.6%	Signal and all backgrounds
Lepton ID/Trigger	✓	1 %	Signal and all backgrounds
Photon ID	✓	1.5 %	Signal and all backgrounds
Pileup	✓	2 %	Signal and all backgrounds
JES	✓	5 %	Signal and all backgrounds
b tagging	✓	2.5 %	Signal and all backgrounds
QCD Scale		0.5 – 25 %	All backgrounds
PDF		2.5 – 10 %	All backgrounds
Control Region Discrepancy	✓	10 – 20 %	Observed data discrepancy in CR1
SR1/CR1 Ratio	✓	1 – 8 %	Shape difference between SR1 and CR1
SR2/SR1 Ratio	✓	10 – 50 %	Shape difference between SR2 and SR1 – only for SR2
SUSY Cross Sections		16 – 28 %	Signal only

5 Results and Interpretation

For systematic uncertainties affecting both the overall rate and shape of the $E_{\mathrm{T}}^{\mathrm{miss}}$ distribution for a given background or signal process, both contributions are treated simultaneously and assumed to be completely correlated. All backgrounds are simulated in MC and assigned systematic uncertainties due to uncertainties in the total integrated luminosity, cross section normalizations due to parton distribution function (PDF) uncertainties and QCD scales, pileup reweighting, and jet energy scales (JES). Trigger and physics object selection efficiencies are assigned a systematic uncertainty due to the uncertainty in the MC scale factors, including b tagging, electron/muon ID and triggers, and photon ID. The systematic uncertainties are summarized in Table 2.

The observed data are compared to the standard model background estimation in $E_{\mathrm{T}}^{\mathrm{miss}}$ in each signal region, across the entire range of $E_{\mathrm{T}}^{\mathrm{miss}}$. The distributions of $E_{\mathrm{T}}^{\mathrm{miss}}$ are shown in Figure 4. Good agreement between prediction and data is observed. The final results are summarized in

Table 3.

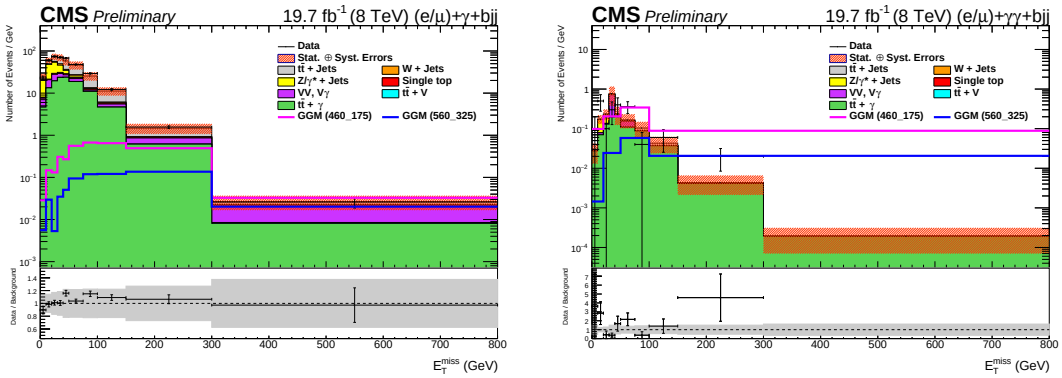

Figure 4: Comparison of data and MC in $E_{\mathrm{T}}^{\mathrm{miss}}$ for the combined (e+μ) signal regions. SR1 (left) with one reconstructed photon and SR2 (right) with two reconstructed photons are shown.

Table 3: Observed data and expected background yields for the combined (e+μ) signal regions. Expectations from two GMSB signal models are included, for which (460_175) refers to $\mathrm{M_{stop}} = 460\,\mathrm{GeV}$ and $\mathrm{M_{bino}} = 175\,\mathrm{GeV}$ and similarly for (560_325). The errors represented below are statistical followed by all systematic uncertainties added in quadrature.

Channel	SR1	SR2
$t\bar{t}$	$1845 \pm 48 \pm 64$	$1.42 \pm 1.31 \pm 0.12$
W/Z + jets	$1100 \pm 43 \pm 35$	$2.12 \pm 1.56 \pm 0.22$
Single t	$130 \pm 14 \pm 6$	–
Diboson	$22.7 \pm 4.9 \pm 1.1$	$0.20 \pm 0.44 \pm 0.06$
$V\gamma$	$431 \pm 25 \pm 116$	$6.2 \pm 2.6 \pm 3.8$
$t\bar{t} + W/Z$	$14.7 \pm 4.0 \pm 1.0$	0.15 ± 0.41
$t\bar{t} + \gamma$	$1926 \pm 47 \pm 388$	$14.0 \pm 4.0 \pm 2.9$
Total Background	$5469 \pm 85 \pm 411$	$24.1 \pm 5.2 \pm 4.8$
GMSB (460_175)	$162 \pm 16 \pm 6$	$87 \pm 12 \pm 2$
GMSB (560_325)	$43.2 \pm 7.5 \pm 1.9$	$18.1 \pm 4.8 \pm 0.6$
Data	5741	30

To interpret the data a GMSB signal spectrum is generated using SuSpect 2.41 [47] with decay tables from SDECAY [48], and NLO cross sections are calculated with PROSPINO [49]. The stop mass (labelled M_{Stop}) is chosen to range from 360 to 910 GeV. The neutralino NLSP ($\tilde{\chi}_1^0$) is assumed for simplicity to be 100% bino-like, and its mass (labelled M_{Bino}) is chosen to range from 150 to 725 GeV. Both masses are stepped in 25 GeV increments for the lowest masses, and in 50 GeV increments elsewhere. All other SUSY particles (squarks, gluinos, and gauginos) are decoupled at very high masses to force the strong production of stop pairs decaying to bino-like NLSPs. The mass region where $\mathrm{M_{Stop}} - \mathrm{M_{Bino}} < M_{\mathrm{top}}$ is not considered as the requirement of high-p_{T} leptons and b jets severely limits sensitivity therein.

Since no significant excess of events beyond the SM expectation is observed, the 95% confidence level (CL) cross section upper limits are calculated combining the results of all four search regions using the $\mathrm{CL_s}$ method [50]. The expected and observed upper limits are shown in Figure 5. The observed cross section upper limits are slightly lower than the expected limits. Observed and expected mass exclusion contours are also determined and shown in Figure 6.

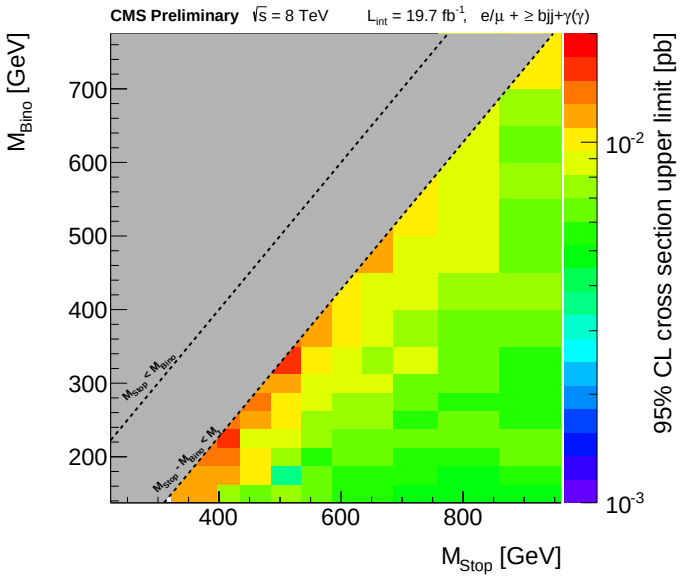

Figure 5: Observed upper cross section CL_s limits at 95% CL in the $M_{Stop} - M_{Bino}$ plane.

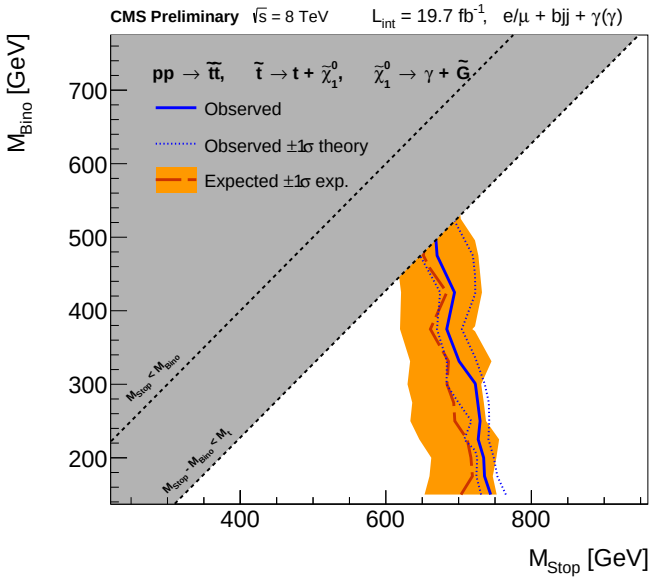

Figure 6: Observed and expected 95% CL exclusion contours for stop and bino masses.

6 Conclusion

We have presented a search for natural gauge-mediated supersymmetry breaking in events with a top quark pair and photons. No significant excess in the shape of the $E_{\mathrm{T}}^{\mathrm{miss}}$ distribution is observed that would indicate the presence of new physics. Cross section upper limits are calculated for a range of stop and bino masses, and stop masses below 650–750 GeV (depending on the bino mass) are excluded. These results set the most stringest exclusion on stop masses in GMSB scenarios available to date.

References

[1] J. Wess and B. Zumino, "Supergauge transformations in four-dimensions", *Nucl. Phys. B* **70** (1974) 39, doi:10.1016/0550-3213(74)90355-1.

[2] Yu. A. Golfand and E. P. Likhtman, "Extension of the Algebra of Poincare Group Generators and Violation of p Invariance", *JETP Lett.* **13** (1971) 323–326. [Pisma Zh. Eksp. Teor. Fiz.13,452(1971)].

[3] D. V. Volkov and V. P. Akulov, "Possible universal neutrino interaction", *JETP Lett.* **16** (1972) 438–440, doi:10.1007/Bfb0105270. [Pisma Zh. Eksp. Teor. Fiz.16,621(1972)].

[4] A. H. Chamseddine, R. L. Arnowitt, and P. Nath, "Locally supersymmetric grand unification", *Phys. Rev. Lett.* **49** (1982) 970, doi:10.1103/PhysRevLett.49.970.

[5] G. L. Kane, C. F. Kolda, L. Roszkowski, and J. D. Wells, "Study of constrained minimal supersymmetry", *Phys. Rev. D* **49** (1994) 6173, doi:10.1103/PhysRevD.49.6173, arXiv:hep-ph/9312272.

[6] P. Fayet, "Supergauge invariant extension of the Higgs mechanism and a model for the electron and its neutrino", *Nucl. Phys. B* **90** (1975) 104, doi:10.1016/0550-3213(75)90636-7.

[7] R. Barbieri, S. Ferrara, and C. A. Savoy, "Gauge models with spontaneously broken local supersymmetry", *Phys. Lett. B* **119** (1982) 343, doi:10.1016/0370-2693(82)90685-2.

[8] L. J. Hall, J. D. Lykken, and S. Weinberg, "Supergravity as the messenger of supersymmetry breaking", *Phys. Rev. D* **27** (1983) 2359, doi:10.1103/PhysRevD.27.2359.

[9] P. Ramond, "Dual theory for free fermions", *Phys. Rev. D* **3** (1971) 2415, doi:10.1103/PhysRevD.3.2415.

[10] CMS Collaboration Collaboration, "Observation of a new boson at a mass of 125 GeV with the CMS experiment at the LHC", *Phys. Lett. B* **716** (2012) 30–61, doi:10.1016/j.physletb.2012.08.021, arXiv:1207.7235.

[11] ATLAS Collaboration, "Observation of a new particle in the search for the Standard Model Higgs boson with the ATLAS detector at the LHC", *Phys. Lett. B* **716** (2012) 1–29, doi:10.1016/j.physletb.2012.08.020, arXiv:1207.7214.

[12] CMS Collaboration, "Precise determination of the mass of the Higgs boson and tests of compatibility of its couplings with the standard model predictions using proton

collisions at 7 and 8 TeV", *Eur. Phys. J. C* **75** (2015), no. 5, 212, doi:10.1140/epjc/s10052-015-3351-7, arXiv:1412.8662.

[13] ATLAS Collaboration, "Measurements of the Higgs boson production and decay rates and coupling strengths using pp collision data at $\sqrt{s} = 7$ and 8 TeV in the ATLAS experiment", *Eur. Phys. J.* **C76** (2016), no. 1, 6, doi:10.1140/epjc/s10052-015-3769-y, arXiv:1507.04548.

[14] ATLAS, CMS Collaboration, "Combined Measurement of the Higgs Boson Mass in pp Collisions at $\sqrt{s} = 7$ and 8 TeV with the ATLAS and CMS Experiments", *Phys. Rev. Lett.* **114** (2015) 191803, doi:10.1103/PhysRevLett.114.191803, arXiv:1503.07589.

[15] J. Barnard, B. Farmer, T. Ghergetta, and M. White, "Natural gauge mediation with a bino NLSP at the LHC", *Phys. Rev. Lett.* **109** (2012) 241801, doi:10.1103/PhysRevLett.109.241801, arXiv:1208.6062.

[16] Y. Kats, P. Meade, M. Reece, and D. Shih, "The Status of GMSB After 1/fb at the LHC", *JHEP* **02** (2012) 115, doi:10.1007/JHEP02(2012)115, arXiv:1110.6444.

[17] R. Barbieri and A. Strumia, "The 'LEP paradox'", in *4th Rencontres du Vietnam: Physics at Extreme Energies (Particle Physics and Astrophysics) Hanoi, Vietnam, July 19-25, 2000*. 2000. arXiv:hep-ph/0007265.

[18] P. Fayet, "Mixing Between Gravitational and Weak Interactions Through the Massive Gravitino", *Phys. Lett. B* **70** (1977) 461, doi:10.1016/0370-2693(77)90414-2.

[19] P. Fayet, "Scattering Cross-Sections of the Photino and the Goldstino (Gravitino) on Matter", *Phys. Lett. B* **86** (1979) 272, doi:10.1016/0370-2693(79)90836-0.

[20] P. Fayet, "Lower Limit on the Mass of a Light Gravitino from e+ e- Annihilation Experiments", *Phys. Lett. B* **175** (1986) 471, doi:10.1016/0370-2693(86)90626-X.

[21] P. Meade, N. Seiberg, and D. Shih, "General Gauge Mediation", *Prog. Theor. Phys. Suppl.* **177** (2009) 143–158, doi:10.1143/PTPS.177.143, arXiv:0801.3278.

[22] M. Buican, P. Meade, N. Seiberg, and D. Shih, "Exploring General Gauge Mediation", *JHEP* **03** (2009) 016, doi:10.1088/1126-6708/2009/03/016, arXiv:0812.3668.

[23] S. Abel, M. J. Dolan, J. Jaeckel, and V. V. Khoze, "Phenomenology of Pure General Gauge Mediation", *JHEP* **12** (2009) 001, doi:10.1088/1126-6708/2009/12/001, arXiv:0910.2674.

[24] R. Barbier et al., "R-parity violating supersymmetry", *Phys. Rept.* **420** (2005) 1, doi:10.1016/j.physrep.2005.08.006, arXiv:hep-ph/0406039.

[25] G. R. Farrar and P. Fayet, "Phenomenology of the production, decay, and detection of new hadronic states associated with supersymmetry", *Phys. Lett. B* **76** (1978) 575, doi:10.1016/0370-2693(78)90858-4.

[26] P. Meade, N. Seiberg, and D. Shih, "General gauge mediation", *Prog. Theor. Phys. Suppl.* **177** (2009) 143, doi:10.1143/PTPS.177.143.

[27] M. Buican, P. Meade, N. Seiberg, and D. Shih, "Exploring general gauge mediation", *JHEP* **03** (2009) 016, doi:10.1088/1126-6708/2009/03/016.

[28] J. T. Ruderman and D. Shih, "General neutralino NLSPs at the early LHC", *JHEP* **08** (2012) 159, doi:10.1007/JHEP08(2012)159, arXiv:1103.6083.

[29] Y. Kats, P. Meade, M. Reece, and D. Shih, "The status of GMSB after 1/fb at the LHC", *JHEP* **02** (2012) 115, doi:10.1007/JHEP02(2012)115, arXiv:1110.6444.

[30] Y. Kats and M. J. Strassler, "Probing colored particles with photons, leptons, and jets", *JHEP* **11** (2012) 097, doi:10.1007/JHEP11(2012)097, arXiv:1204.1119.

[31] P. Grajek, A. Mariotti, and D. Redigolo, "Phenomenology of general gauge mediation in light of a 125 GeV Higgs", *JHEP* **07** (2013) 109, doi:10.1007/JHEP07(2013)109, arXiv:1303.0870.

[32] CMS Collaboration, "Performance of Photon Reconstruction and Identification with the CMS Detector in Proton-Proton Collisions at sqrt(s) = 8 TeV", *JINST* **10** (2015), no. 08, P08010, doi:10.1088/1748-0221/10/08/P08010, arXiv:1502.02702.

[33] CMS Collaboration, "The CMS experiment at the CERN LHC", *JINST* **3** (2008) S08004, doi:10.1088/1748-0221/3/08/S08004.

[34] CMS Collaboration Collaboration, "Particle-Flow Event Reconstruction in CMS and Performance for Jets, Taus, and MET", Technical Report CMS-PAS-PFT-09-001, CERN, 2009. Geneva, Apr, 2009.

[35] CMS Collaboration Collaboration, "Commissioning of the Particle-flow Event Reconstruction with the first LHC collisions recorded in the CMS detector", Technical Report CMS-PAS-PFT-10-001, CERN, 2010, 2010.

[36] CMS Collaboration Collaboration, "Commissioning of the Particle-Flow reconstruction in Minimum-Bias and Jet Events from pp Collisions at 7 TeV", Technical Report CMS-PAS-PFT-10-002, CERN, Geneva, 2010.

[37] M. Cacciari, G. P. Salam, and G. Soyez, "The anti-k_T jet clustering algorithm", *JHEP* **04** (2008) 063, doi:10.1088/1126-6708/2008/04/063, arXiv:0802.1189.

[38] M. Cacciari, G. P. Salam, and G. Soyez, "FastJet user manual", *Eur. Phys. J. C* **72** (2012) 1896, doi:10.1140/epjc/s10052-012-1896-2, arXiv:1111.6097.

[39] CMS Collaboration, "Performance of CMS muon reconstruction in pp collision events at $\sqrt{s} = 7$ TeV", *JINST* **7** (2012) P10002, doi:10.1088/1748-0221/7/10/P10002, arXiv:1206.4071.

[40] S. Baffioni et al., "Electron reconstruction in CMS", *Eur. Phys. J. C* **49** (2007), no. 4, 1099–1116, doi:10.1140/epjc/s10052-006-0175-5.

[41] CMS Collaboration Collaboration, "Algorithms for b Jet identification in CMS", Technical Report CMS-PAS-BTV-09-001, CERN, 2009. Geneva, Jul, 2009.

[42] J. Alwall et al., "MadGraph 5: going beyond", *JHEP* **06** (2011) 128, doi:10.1007/JHEP06(2011)128, arXiv:1106.0522.

[43] T. Sjöstrand, S. Mrenna, and P. Z. Skands, "PYTHIA 6.4 physics and manual", *JHEP* **05** (2006) 026, doi:10.1088/1126-6708/2006/05/026, arXiv:hep-ph/0603175.

[44] S. Frixione, P. Nason, and C. Oleari, "Matching NLO QCD computations with Parton Shower simulations: the POWHEG method", *JHEP* **0711** (2007) 070, doi:10.1088/1126-6708/2007/11/070, arXiv:0709.2092.

[45] Z. Was, "TAUOLA the library for tau lepton decay, and KKMC / KORALB / KORALZ /... status report", *Nucl.Phys.Proc.Suppl.* **98** (2001) 96–102, doi:10.1016/S0920-5632(01)01200-2, arXiv:hep-ph/0011305.

[46] R. Field, "Min-Bias and the Underlying Event at the LHC", *Acta Phys.Polon. B* **42** (2011) 2631–2656, doi:10.5506/APhysPolB.42.2631, arXiv:1110.5530.

[47] A. Djouadi, J.-L. Kneur, and G. Moultaka, "SuSpect: A Fortran code for the supersymmetric and Higgs particle spectrum in the MSSM", *Comput.Phys.Commun.* **176** (2007) 426–455, doi:10.1016/j.cpc.2006.11.009, arXiv:hep-ph/0211331.

[48] M. Mühlleitner, A. Djouadi, and Y. Mambrini, "SDECAY: a Fortran code for the decays of the supersymmetric particles in the {MSSM}", *Computer Physics Communications* **168** (2005), no. 1, 46 – 70, doi:http://dx.doi.org/10.1016/j.cpc.2005.01.012.

[49] W. Beenakker, R. Hopker, and M. Spira, "PROSPINO: A Program for the production of supersymmetric particles in next-to-leading order QCD", arXiv:hep-ph/9611232.

[50] "Proceedings of the First Workshop on Confidence Limits", in *Workshop on confidence limits, CERN, Geneva, Switzerland, 17-18 Jan 2000: Proceedings*, F. James, Y. Perrin, and L. Lyons, eds., CERN. CERN, Geneva, 2000. doi:10.5170/CERN-2000-005.